AIAA JOURNAL
Vol. 31, No. 4, April 1993

In-Plane Response of Laminates with Spatially Varying Fiber Orientations: Variable Stiffness Concept

Zafer Gürdal* and Reynaldo Olmedo†
Virginia Polytechnic Institute and State University, Blacksburg, Virginia 24061

A solution to the plane elasticity problem for a symmetrically laminated composite panel with spatially varying fiber orientations has been obtained. The fiber angles vary along the length of the composite laminate, resulting in stiffness properties that change as a function of location. This work presents an analysis of the stiffness variation and its effects on the elastic response of the panel. The in-plane response of a variable stiffness panel is governed by a system of coupled elliptic partial differential equations. Solving these equations yields the displacement fields, from which the strains, stresses, and stress resultants can be subsequently calculated. A numerical solution has been obtained using an iterative collocation technique. Corresponding closed-form solutions are presented for three sets of boundary conditions, two of which have exact solutions, and therefore serve to validate the numerical model. The effects of the variable fiber orientation on the displacement fields, stress resultants, and global stiffness are analyzed.

Introduction

COMPOSITE materials have gained prominence by allowing the designer to tailor a structure to provide the best static and dynamic response under the prescribed loads. For years the tailoring of these structures has been done by varying the orientation of straight fiber prepregs or the total thickness of the laminate. Recent developments in manufacturing techniques, such as computer controlled three-axes filament winding, tape-laying machines, and fiber and tow placement technology, make it possible to fabricate composite structures with fiber orientations that vary from one location to another. For flat panels, varying the orientation of the fibers along the plate axes results in a curved fiber format, which exhibits variable stiffness properties.

The current literature has only a handful of works on the analysis of panels with variable stiffness properties. Using the Ritz method, Martin and Leissa[1] have successfully modeled a composite sheet with a variable fiber volume fraction. They have shown that improvements in buckling performance are possible using the variable stiffness concept. In addition, Kuo et al.[2] have successfully manufactured and modeled elastomer composite sheets having fibers in the form of sinusoidal waves. For rectangular laminated panels with a central hole, Hyer and Lee[3] have developed finite element models of panels with curvilinear fiber format to improve strength and buckling performance. By varying the fiber angle from one element to another, an approximation to a curvilinear fiber format is obtained, and based on the distribution of the internal stresses, improvements in the failure load over straight fiber configurations are achieved. Finally, DiNardo and Lagace[4] have found that for panels with dropped internal plies, the buckling performance is driven by the changes in stiffness along the panel.

The motivation for this work is to model the in-plane elastic response of panels having a curved fiber format, with the intention of subsequently extending the analysis to encompass the buckling response, where improvements over current configurations are likely. A continious curved fiber format is proposed to eliminate some of the problems encountered in some of the studies just mentioned, namely, the issue of manufacturability, continuity of the fibers or the fiber volume fraction, and stress concentration due to abrupt changes in thickness.

The scope of this study is limited to the in-plane response of square panels for which the fiber angle varies as a function of one spatial coordinate. An analysis of the stiffness distribution for various configurations is presented first. The governing equations are then derived, and a numerical technique for their solution is introduced. Three sets of boundary conditions are identified, and closed-form solutions are developed for each case.

Analysis

Constitutive Relations

Applying the classical lamination theory to panels with variable fiber angles results in A, B, and D matrices in the constitutive relation

$$\begin{Bmatrix} N \\ M \end{Bmatrix} = \begin{bmatrix} A & B \\ B & D \end{bmatrix} \begin{Bmatrix} \epsilon \\ \kappa \end{Bmatrix} \tag{1}$$

that do not have constant values [i.e., $A = A(x, y)$] and thus reflect the changes in the fiber angle. The vectors N and M represent the stress resultant forces and moments; and ϵ and κ denote the midplane strains and curvatures, respectively. Using the material invariants[5] for an orthotropic lamina, U_1, U_2, . . . , U_5 a convenient form of the A, B, and D matrices of a laminate is obtained as

$$[A, B, D] = \begin{bmatrix} e_{11} & e_{12} & e_{16} \\ & e_{22} & e_{26} \\ \text{(symm)} & & e_{66} \end{bmatrix} \tag{2}$$

where the elements e_{ij} are defined by

$$e_{11} = U_1V_0 + U_2V_1 + U_3V_3 \tag{3a}$$

$$e_{12} = U_4V_0 - U_3V_3 \tag{3b}$$

$$e_{16} = -\tfrac{1}{2}U_2V_2 - U_3V_4 \tag{3c}$$

$$e_{22} = U_1V_0 - U_2V_1 + U_3V_3 \tag{3d}$$

Received March 13, 1992; presented as Paper 92-2472 at the AIAA/ASME/ASCE/AHS/ASC 33rd Structures, Structural Dynamics, and Materials Conference, Dallas, TX, April 13–15, 1992; revision received Sept. 1, 1992; accepted for publication Sept. 14, 1992.

*Associate Professor, Department of Engineering Science and Mechanics. Senior Member AIAA.

†Graduate Research Assistant, Department of Engineering Science and Mechanics. Student Member AIAA.

$$e_{26} = -\tfrac{1}{2}U_2V_2 + U_3V_4 \tag{3e}$$

$$e_{66} = U_5V_0 - U_3V_3 \tag{3f}$$

and where the V are defined by

$$V_{0(A,\,B,\,D)} = \left[h,\ 0,\ \frac{h^3}{12}\right] \tag{4a}$$

$$V_{1(A,\,B,\,D)} = \int_{-h/2}^{h/2} \cos(2\theta)[1,\ z,\ z^2]\,dz \tag{4b}$$

$$V_{2(A,\,B,\,D)} = \int_{-h/2}^{h/2} \sin(2\theta)[1,\ z,\ z^2]\,dz \tag{4c}$$

$$V_{3(A,\,B,\,D)} = \int_{-h/2}^{h/2} \cos(4\theta)[1,\ z,\ z^2]\,dz \tag{4d}$$

$$V_{4(A,\,B,\,D)} = \int_{-h/2}^{h/2} \sin(4\theta)[1,\ z,\ z^2]\,dz \tag{4e}$$

and h is the total thickness of the laminate. Limiting the stacking sequence to symmetric balanced laminates, $[\pm\theta]_s$, the extensional stiffness matrix A reduces to

$$A = h\begin{bmatrix} U_1 & U_4 & 0 \\ U_4 & U_1 & 0 \\ 0 & 0 & U_5 \end{bmatrix} + h\begin{bmatrix} U_2 & 0 & 0 \\ 0 & -U_2 & 0 \\ 0 & 0 & 0 \end{bmatrix}\cos(2\theta)$$

$$+h\begin{bmatrix} U_3 & -U_3 & 0 \\ -U_3 & U_3 & 0 \\ 0 & 0 & -U_3 \end{bmatrix}\cos(4\theta) \tag{5}$$

where the fiber angle θ is a function of the location in the panel, $\theta = \theta(x, y)$. For a balanced symmetric laminate $\boldsymbol{B} = \mathbf{0}$, and the in-plane constitutive relation simplifies to

$$\begin{Bmatrix} N_x \\ N_y \\ N_{xy} \end{Bmatrix} = \begin{bmatrix} A_{11} & A_{12} & 0 \\ A_{12} & A_{22} & 0 \\ 0 & 0 & A_{66} \end{bmatrix}\begin{Bmatrix} \epsilon_x \\ \epsilon_y \\ \gamma_{xy} \end{Bmatrix} \tag{6}$$

There are several ways to vary the fiber angle. However, as a consequence of practical limitations on processing techniques that result in fiber patterns that are parallel to one another, the fiber orientation is made to vary only along one of the coordinates. A linear variation of the fiber orientation along the x coordinate is obtained if the fiber orientation is defined by

$$\theta(x) = \frac{2(T_1 - T_0)}{a}x + T_0 \tag{7}$$

The fiber angle starts from the angle T_0 at the panel midlength $x = 0$, and reaches a value of T_1 at the panel end $x = a/2$. The fiber orientation is assumed to be symmetric with respect to $x = 0$. Thus, a fiber path that passes through the origin is a smooth antisymmetric function of the x coordinate, defined by

$$y = \frac{a}{2(T_1 - T_0)}\left\{-\ell n\left[\cos\left(T_0 + \frac{2(T_1 - T_0)x}{a}\right)\right] + \ell n[\cos(T_0)]\right\}$$

$$0 \le x < a/2 \tag{8a}$$

$$y = \frac{a}{2(T_1 - T_0)}\left\{\ell n\left[\cos\left(T_1 + \frac{2(T_1 - T_0)x}{a}\right)\right] - \ell n[\cos(T_1)]\right\}$$

$$-a/2 \le x < 0 \tag{8b}$$

Although at the outset the limitations on the fiber orientations may look too restrictive, it is possible to generate panels with a wide range of properties. For example, some of the panel laminations are presented in Fig. 1 for various linear combinations of the panel midlength and panel end angles, T_0 and T_1.

Note that a panel with $T_0 = T_1 = 45$ deg is actually a panel with straight fibers and has constant stiffness properties along the length. In addition, other fiber angle orientations are possible, such as sinusoidal fiber patterns defined by

$$y = \chi \sin\left(\frac{2\pi x}{\lambda}\right) \tag{9}$$

However, the fiber angle defined in Eq. (7) lends itself to the development of closed-form solutions for the in-plane response.

An effective axial modulus and Poisson's ratio of a laminated orthotropic material are defined by

$$E_x(x) = \frac{A_{11}A_{22} - A_{12}^2}{hA_{22}}, \qquad \nu_{xy}(x) = \frac{A_{12}}{A_{22}} \tag{10}$$

For straight fiber format panels these quantities are constant for the entire panel, but for a variable stiffness panel the A are functions of x; therefore, $E_x = E_x(x)$ and $\nu_{xy} = \nu_{xy}(x)$ do not represent global values but, rather, a local stiffness and Poisson's ratio. The normalized x direction modulus $E_x(x)$ is shown in Fig. 2 as a function of the x coordinate for $T_0 = 45$ deg and values of T_1 ranging from 0 to 45 deg. For an angle change of only 15 deg ($T_1 = 30$ deg) the axial stiffness at the panel end is about two times greater than at the panel midlength. A more drastic change is seen when $T_1 = 0$ deg, since the effective stiffness at the panel end is almost seven times greater than at the panel midlength. The opposite may be

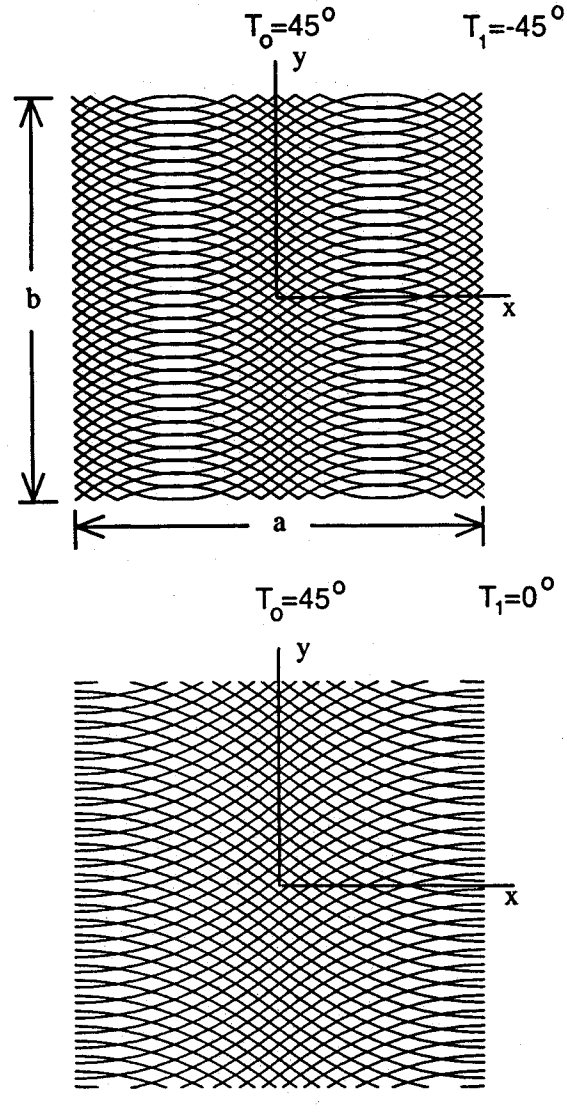

Fig. 1 Variable stiffness configurations [($\pm\theta$) layers shown].

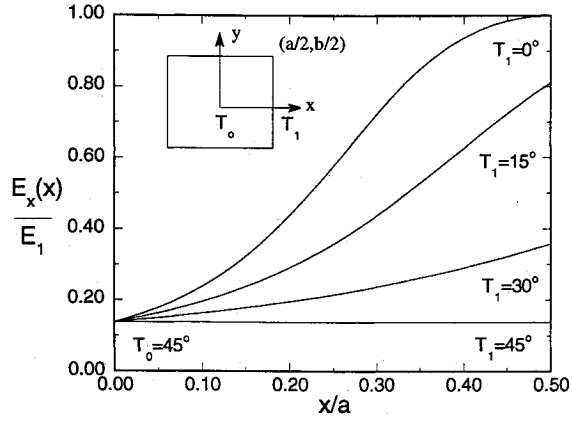

Fig. 2 Effective x direction modulus as a function of x/a.

accomplished by having T_1 greater than T_0. The line for $T_1 = 45$ deg represents a panel with straight fibers.

Under uniaxial x-direction compression, the transverse displacement v and stress resultant N_y will be affected by the changes in $\nu_{xy}(x)$. The ν_{xy} is shown as a function of the x coordinate in Fig. 3 for a panel with $T_0 = 45$ deg. When $T_1 = 30$ deg the effective Poission's ratio increases almost linearly with respect to the normalized coordinate x/a. The curves for $T_1 = 0$ deg and $T_1 = 15$ deg show that $\nu_{xy}(x)$ will reach a maximum at $x/a = 0.23$ and $x/a = 0.35$, respectively. Note that at $x = a/2$ the value of $\nu_{xy}(x)$ for the $T_1 = 0$-deg curve is given by the material property $\nu_{12} = 0.28$, since the fibers are all oriented at a 0-deg angle. Given that the fiber orientations are functions of the x coordinate only, $E_x(x)$ and $\nu_{xy}(x)$ do not change in the y direction in this case.

Equilibrium Equations

The in-plane plate equilibrium equations are given by

$$\frac{\partial N_x}{\partial x} + \frac{\partial N_{xy}}{\partial y} = 0 \tag{11a}$$

$$\frac{\partial N_y}{\partial y} + \frac{\partial N_{xy}}{\partial x} = 0 \tag{11b}$$

By substituting the in-plane constitutive equations defined in Eq. (6) and the linear strain-displacement relationships

$$\epsilon_x = \frac{\partial u}{\partial x}, \qquad \epsilon_y = \frac{\partial v}{\partial y}, \qquad \gamma_{xy} = \frac{\partial u}{\partial y} + \frac{\partial v}{\partial x} \tag{12}$$

into the in-plane equilibrium Eqs. (11a) and (11b) yields

$$A_{11}(x)\frac{\partial^2 u}{\partial x^2} + A_{66}(x)\frac{\partial^2 u}{\partial y^2} + [A_{12}(x) + A_{66}(x)]\frac{\partial^2 v}{\partial x \partial y} + \frac{\partial A_{11}(x)}{\partial x}\frac{\partial u}{\partial x} + \frac{\partial A_{12}(x)}{\partial x}\frac{\partial v}{\partial y} = 0 \tag{13a}$$

$$A_{66}(x)\frac{\partial^2 v}{\partial x^2} + A_{22}(x)\frac{\partial^2 v}{\partial y^2} + [A_{12}(x) + A_{66}(x)]\frac{\partial^2 u}{\partial x \partial y} + \frac{\partial A_{66}(x)}{\partial x}\left(\frac{\partial u}{\partial y} + \frac{\partial v}{\partial x}\right) = 0 \tag{13b}$$

where the A_{ij} are given by Eq. (5) and $\theta = \theta(x)$. Note that since the symmetric laminate is assumed to be balanced, the A_{16} and A_{26} terms are identically zero. The equilibrium equations form a set of coupled elliptic partial differential equations with variable coefficients. Their solution yields the u and v displacement fields, from which the strains can be calculated. The constitutive equations can then be applied to obtain the in-plane stress resultants.

Solution

The displacement fields for variable stiffness panels can be quite complex, yielding nonuniform strain and stress fields. In contrast to panels with straight fibers, where a homogeneous in-plane stress state automatically satisfies the equilibrium Eqs. (11a) and (11b), the complexity of the governing equations for variable stiffness configurations precludes such simple solutions. Two approaches are presented for the solution of the displacements. The first approach is a numerical scheme that can be applied to generic problems governed by partial differential equations in the form of Eqs. (13). The second approach is an attempt to find computationally efficient closed-form solutions. The angles T_0 and T_1 have been chosen to range between 0 and 45 deg. The results presented here are based on a four-layer graphite-epoxy laminate having $E_1 = 26.25 \times 10^6$ psi, $E_2 = 1.49 \times 10^6$ psi, $G_{12} = 1.04 \times 10^6$ psi, and $\nu_{12} = 0.28$, with a layer thickness of 0.005 in. (hence, $h = 0.02$ in.). The panels are square, $a = b = 10$ in. Because of the twofold symmetry of the problem, only one-quarter of the panel was modeled. All panels have linear fiber angle variations.

Numerical Solution

Equations (13a) and (13b) can be rearranged in the following form:

$$A_{11}(x)\frac{\partial^2 u}{\partial x^2} + A_{66}(x)\frac{\partial^2 u}{\partial y^2} + \frac{\partial A_{11}(x)}{\partial x}\frac{\partial u}{\partial x} = p(x, y) \tag{14a}$$

$$A_{66}(x)\frac{\partial^2 v}{\partial x^2} + A_{22}(x)\frac{\partial^2 v}{\partial y^2} + \frac{\partial A_{66}(x)}{\partial x}\frac{\partial v}{\partial x} = q(x, y) \tag{14b}$$

where

$$p(x, y) = -[A_{12}(x) + A_{66}(x)]\frac{\partial^2 v}{\partial x \partial y} - \frac{\partial A_{12}(x)}{\partial x}\frac{\partial v}{\partial y} \tag{15}$$

and

$$q(x, y) = -[A_{12}(x) + A_{66}(x)]\frac{\partial^2 u}{\partial x \partial y} - \frac{\partial A_{66}(x)}{\partial x}\frac{\partial u}{\partial y} \tag{16}$$

Equations (14) form a system of nonhomogeneous partial differential equations with variable coefficients. The coupling between the in-plane displacements u and v occurs through the nonhomogeneous terms $p(x, y)$ and $q(x, y)$. The equations cannot be decoupled; therefore, to obtain a numerical solution, an iterative technique is necessary. The numerical solution of such elliptic boundary value problems has been studied extensively[6] and the ELLPACK[7] elliptic differential equation solver was found to perform well for this particular problem. A method of solution used by ELLPACK, Hermite collocation, involves approximating each displacement field by a Hermite bicubic piecewise polynomial $\alpha(x, y)$ over a rectangular grid containing four $NGRX \times NGRY$ Gauss points, where

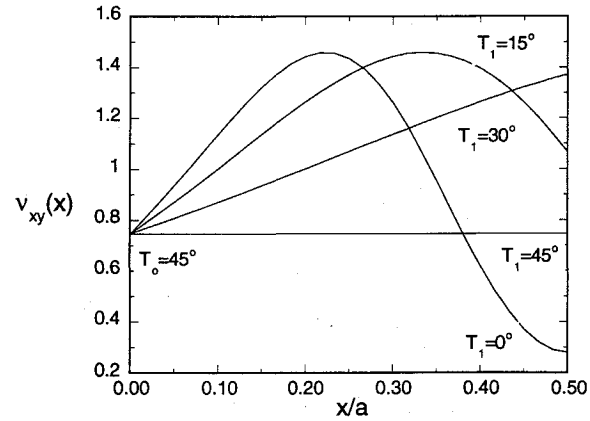

Fig. 3 Effective Poisson's ratio as a function of x/a.

NGRX and *NGRY* are the number of x and y grid lines, respectively. The form of the approximation is given by

$$\alpha(x, y) = \sum_{k=1}^{NGRX} \sum_{j=1}^{NGRY} \{a_{k,j}h_k(x)h_j(y) + b_{k,j}h_k(x)g_j(y) + c_{k,j}g_k(x)h_j(y) + d_{k,j}g_k(x)g_j(y)\} \quad (17)$$

where $h_k(x)$ and $g_k(x)$ are the Hermite cubic basis functions.[7] The differential equation is satisfied at the interior Gauss points and along the boundary under the prescribed boundary conditions, resulting in four $NGRX \times NGRY$ equations for the coefficients $a_{k,j}$, $b_{k,j}$, $c_{k,j}$, and $d_{k,j}$. The iterative solution of the system begins with an assumed solution for the v displacement field, which is then used to obtain $p(x, y)$, so that $u(x, y)$ may be obtained by solving Eq. (14a). The new u then becomes the input for $q(x, y)$ in Eq. (14b), and a new solution for v is obtained. The control program iterates, alternating between the two equations until the solutions converge. Once the displacement fields are obtained, the strains and stress resultants can be calculated using the strain-displacement and constitutive relations.

Closed-Form Solutions

Closed-form solutions are now developed for three distinct cases. The boundary conditions for each case are shown in Fig. 4. Since only one-quarter of the panel is modeled, the boundary conditions at $x = 0$ and $y = 0$ represent symmetry conditions. The symmetry conditions with respect to the x and y axes are $v = \partial u/\partial y = 0$ and $u = \partial v/\partial x = 0$, respectively. In all cases the panel is loaded by a uniform end shortening, u_0, applied at $x = a/2$, but the boundary conditions along the transverse edges are different. Under the boundary conditions for case I the transverse edges are traction free. Case II represents a panel with fixed transverse edges. Under boundary conditions for the third case, the transverse edges are allowed to move freely, but they are forced to remain straight. Hence, one of the conditions on the moveable straight edge is an integral condition that the total load at $y = b/2$ must be zero. For a panel with straight fibers, cases I and III would be identical; however, since the deformation patterns of variable stiffness panels are nonuniform, case III represents a distinct case.

Case I

Whereas an exact closed-form solution cannot be obtained for this case, an approximate solution may be derived under certain assumptions. For straight fiber panels the solution is simple, $N_y(x, y) = 0$, $N_{xy}(x, y) = 0$, and N_x is a constant. Assuming that the same is true for variable stiffness panels, N_y from Eq. (6) can be used to express the transverse strain in terms of the axial strain as

$$\frac{\partial v}{\partial y} = -\frac{A_{12}(x)}{A_{22}(x)} \frac{\partial u}{\partial x} \quad (18)$$

Assuming that the axial stress resultant N_x is constant everywhere in the panel ($N_x = N_0$), substituting Eqs. (5) and (18) into N_x from Eq. (6), and solving for the axial strain yields

$$\frac{\partial u}{\partial x} = \frac{2N_0[U_1 - U_2\cos(2\theta) + U_3\cos(4\theta)]}{h[2U_1^2 - U_2^2 - 2U_4^2 + (U_2^2 + 4U_1U_3 + 4U_3U_4)\cos(4\theta)]} \quad (19)$$

where the fiber angle θ is a function of x given by Eq. (7), and the denominator has been simplified using trigonometric identities. Since the stiffness changes only in the x direction, the u displacement can be assumed to be a function of the x coordinate only. Integration of Eq. (19) with respect to x results in the closed-form expression for the u displacement. For a linear angle variation, the u displacement field consists of four parts plus a constant of integration as

$$u(x) = u_1(x) + u_2(x) + u_3(x) + u_4(x) + u_r \quad (20)$$

where

$$u_1(x) = \frac{-aN_0U_1 \tan^{-1}\left\{\dfrac{(C_2 - C_1)\tan[2\theta(x)]}{\sqrt{C_1^2 - C_2^2}}\right\}}{2\sqrt{C_1^2 - C_2^2}(T_0 - T_1)h} \quad (21a)$$

$$u_2(x) = \frac{aN_0U_2 \tan^{-1}\left\{\dfrac{2C_2 \sin[2\theta(x)]}{\sqrt{-2(C_1C_2 + C_2^2)}}\right\}}{2\sqrt{-2(C_1C_2 + C_2^2)}(T_0 - T_1)h} \quad (21b)$$

$$u_3(x) = \frac{aN_0U_2\theta(x)}{C_2(T_0 - T_1)h} \quad (21c)$$

$$u_4(x) = \frac{aN_0U_3C_1 \tan^{-1}\left\{\dfrac{(C_2 - C_1)\tan[2\theta(x)]}{\sqrt{C_1^2 - C_2^2}}\right\}}{2C_2\sqrt{C_1^2 - C_2^2}(T_0 - T_1)h} \quad (21d)$$

and where

$$C_1 = 2U_1^2 - U_2^2 - 2U_4^2 \quad (22a)$$

$$C_2 = 4U_1U_3 + 4U_3U_4 - U_2^2 \quad (22b)$$

The constant of integration u_r can be evaluated by suppressing the rigid body motion of the panel. Equation (20) may be used to solve for N_0 given the prescribed end displacement u_0 at $x = a/2$. The v displacement field is then given by

$$v(x, y) = \frac{-2N_0\{U_4 - U_3\cos[4\theta(x)]\}y}{h\{C_1 + C_2\cos[4\theta(x)]\}} \quad (23)$$

which is obtained by integrating Eq. (18) with respect to y.

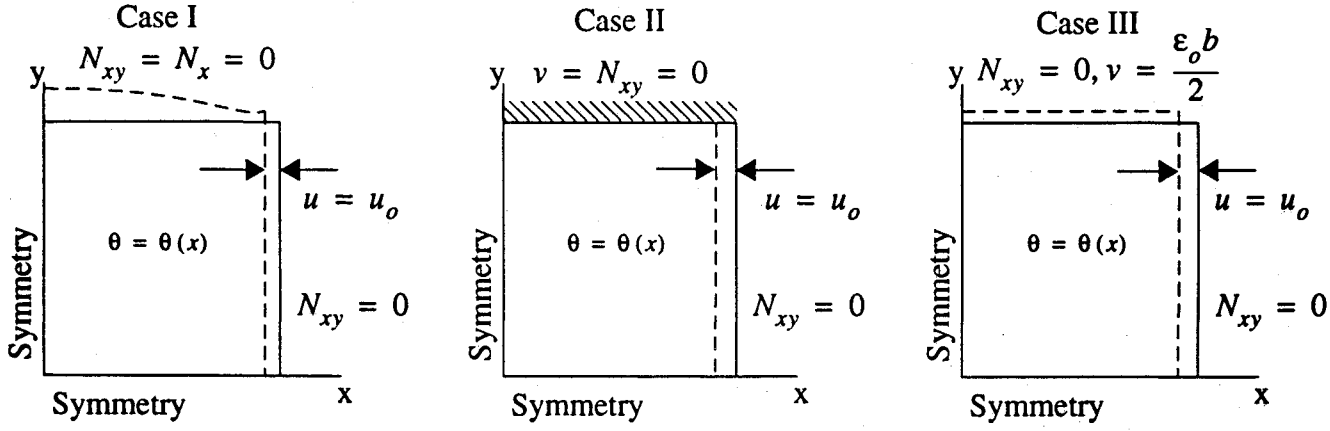

Fig. 4 Quarter panel boundary conditions for each case.

Case II

When the v displacement of the transverse edges ($y = \pm b/2$) is fixed, an exact solution for the u displacement field and stress resultants can be obtained. The boundary conditions for this case are illustrated in Fig. 4. A solution of the form, $N_x = N_0$, $N_{xy} = 0$, and $\epsilon_y = 0$, where N_0 is a constant, satisfies the equilibrium equations and boundary conditions. The v displacement field is identically zero everywhere. Therefore, solving Eq. (6) for the axial strain yields

$$\frac{\partial u}{\partial x} = \frac{N_0}{A_{11}} \tag{24}$$

The transverse stress resultant can be calculated from Eq. (6) as

$$N_y = \frac{A_{12}N_0}{A_{11}} \tag{25}$$

By integrating Eq. (24) we obtain the axial displacement field

$$u = \int \frac{N_0}{A_{11}}\,dx + f(y) \tag{26}$$

By inspection, $f(y)$ must be identically zero in order to satisfy Eqs. (13a) and (13b). Mathematica,[8] a mathematics symbolic manipulation program, was used to carry out the algebraic operations to find the u displacement field. Substituting for A_{11} from Eq. (5), results in

$$u(x) = \int \frac{N_0}{h[U_1 + U_2\cos(2\theta) + U_3\cos(4\theta)]}\,dx + C \tag{27}$$

where $\theta = \theta(x)$. The integration can be carried out by first changing the integration variable to θ using Eq. (7) and then rewriting the cosine terms in their complex exponential form. Using the variable transformation $t = e^{2i\theta}$, and letting

$$\rho = \frac{N_0 a}{2ihU_3(T_1 - T_0)} \tag{28}$$

the integral becomes

$$u(t) = \rho \int \frac{t\,dt}{t^4 + (2U_1/U_3)t^2 + (U_2/U_3)(t^3 + t) + 1} \tag{29}$$

This integral may now be evaluated using a partial fraction expansion

$$u(t) = \rho \int \frac{q_1}{t - t_1} + \frac{q_2}{t - t_2} + \frac{q_3}{t - t_3} + \frac{q_4}{t - t_4}\,dt + C \tag{30}$$

where the roots, $t_1, \ldots, t_4$ are given by

$$t_1 = \tfrac{1}{2}[\sqrt{-4 + (-\omega + \phi)^2} + \omega - \phi] \tag{31a}$$

$$t_2 = \tfrac{1}{2}[-\sqrt{-4 + (-\omega + \phi)^2} + \omega - \phi] \tag{31b}$$

$$t_3 = \tfrac{1}{2}[\sqrt{-4 + (\omega + \phi)^2} - \omega - \phi] \tag{31c}$$

$$t_4 = \tfrac{1}{2}[-\sqrt{-4 + (\omega + \phi)^2} - \omega - \phi] \tag{31d}$$

where

$$\omega = \sqrt{2 + \frac{U_2^2}{4U_3^2} - \frac{2U_1}{U_3}}, \qquad \phi = \frac{U_2}{2U_3} \tag{32}$$

The values of the q_j are obtained by solving the linear system of equations that results from the partial fraction expansion.

Finally, the integral is obtained as

$$u(x) = \frac{N_0 a}{2ihU_3(T_1 - T_0)} \sum_{j=1}^{4} q_j \ln(e^{2i\theta} - t_j) + C \tag{33}$$

where $\theta = \theta(x)$ and the constant C is found by suppressing the rigid body motion of the panel. In this case, the N_x stress resultant remains constant, and the u displacement field is not linear.

Case III

When a variable stiffness panel is loaded under the boundary conditions for case I, the transverse edges do not remain straight. Instead, they bow when the panel is compressed. It is conceivable that by attaching stiffeners that have large in-plane bending stiffnesses, the transverse edges of a variable stiffness panel may be allowed to move freely but be required to remain straight. The boundary conditions for this case are shown as case III in Fig. 4. The requirement that the integral of N_y along the panel length be identically zero ensures that the net transverse load being applied is zero. For this case, $N_x = N_0$, $N_{xy} = 0$, $v = \epsilon_0 y$, and $\epsilon_y = \epsilon_0$, where N_0 and ϵ_0 are constants. The transverse stress resultant is given by

$$N_y = \frac{A_{12}N_0}{A_{11}} + \frac{A_{22}A_{11} - A_{12}^2}{A_{11}}\epsilon_0 \tag{34}$$

The integral of N_y at $y = b/2$ along the x direction is given by

$$P_y = \int_0^{a/2} N_y(x, b/2)\,dx = cN_0 + d\epsilon_0 = 0 \tag{35}$$

where

$$c = \int_0^{a/2} \frac{A_{12}}{A_{11}}\,dx, \qquad d = \int_0^{a/2} \frac{A_{22}A_{11} - A_{12}^2}{A_{11}}\,dx \tag{36}$$

The integrals can be evaluated by using the transformation and partial fraction technique described for case II. The transverse strain that satisfies the integral condition for a given load N_0 is, therefore, given by

$$\epsilon_0 = -(cN_0/d) \tag{37}$$

By using Eq. (6), the axial strain is

$$\frac{\partial u}{\partial x} = \frac{N_0}{A_{11}} - \frac{A_{12}\epsilon_0}{A_{11}} \tag{38}$$

Integration of this expression with respect to x yields the u displacement as

$$u(x) = \frac{-iN_0 a}{2(T_1 - T_0)} \left\{ \frac{1}{U_3 h} \sum_{j=1}^{4} q_j \ln(e^{2i\theta} - t_j) - \frac{c}{2d} \sum_{j=1}^{5} q_j' \ln(e^{2i\theta} - t_j') \right\} + C \tag{39}$$

where, the q_j and t_j are the same as in case II; the t_j', which are the roots of the second term, are the same as in case II, but include the additional root $t_5' = 0$. The q_j' are the coefficients from the partial fraction expansion of the second term. The constant C is evaluated by suppressing the rigid body motion of the panel.

Results

The elastic response of the variable stiffness panels was analyzed both by using a numerical model and by using the closed-form solutions. First, an adequate grid and convergence criterion was established for the numerical solution. Since the transverse stress resultant N_y must be zero at $y = b/2$ for case I, the size of a uniform square $N \times N$ grid was chosen on the basis of how well this condition was satisfied. With a 10×10 grid, the ratio of N_x/N_y along the upper boundary, away from the boundary collocation points, is less than 10^{-4}, and the displacements are converged to four significant figures. Therefore, a 10×10 grid was deemed adequate for the analysis of the variable stiffness panels.

Since an iterative procedure is used for the solution of the coupled equations, a convergence criterion is necessary. The convergence criterion is given as follows:

$$\left|\frac{u_k}{u_{k-1}} - 1\right| < 10^{-6}, \qquad \left|\frac{v_k}{v_{k-1}} - 1\right| < 10^{-6} \tag{40}$$

where k is the iteration number. Equation (40) was applied at 200 points in the panel, and the program continued to iterate until the condition was satisfied at every point.

Case I: Free Transverse Edges

An approximate closed-form solution was derived for this case under two important assumptions: the transverse stress resultant N_y was assumed to be zero, and N_x was assumed to be constant throughout the plate. The validity of these assumptions was analyzed by comparing the results obtained based on the approximate solution with the numerical results obtained using Hermite collocation.

Because of the change in stiffness, loading a variable stiffness panel with a prescribed end load ($N_x = N_0$) will yield a different elastic response compared to the response obtained with a constant end shortening u_0. In addition, the displacement fields are different from the displacement fields for laminates with straight fibers; that is, the u and v displacements are not linear with respect to x and y, respectively. Shown in Fig. 5 is the variation of u as a function of x when $y = 0$ and $y = b/2$ for a panel with $T_0 = 45$ deg and $T_1 = 0$ deg. For this case, the pattern is clearly nonlinear. The axial strain, given by the slope of the curve in Fig. 5, is highest in the more compliant part of the panel, close to $x = 0$. At $x = a/2$, where the axial stiffness is higher, the axial strain is smaller. Note the difference between the curves for $y = 0$ and for $y = b/2$, indicating that u and, therefore, ϵ_x are a function of both x and y. A similar effect is found in the v displacement, which varies due to changes in $\nu_{xy}(x)$.

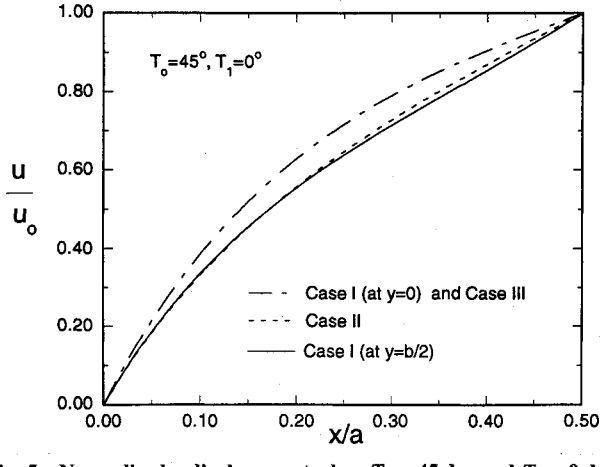

Fig. 5 Normalized u displacement when $T_0 = 45$ deg and $T_1 = 0$ deg.

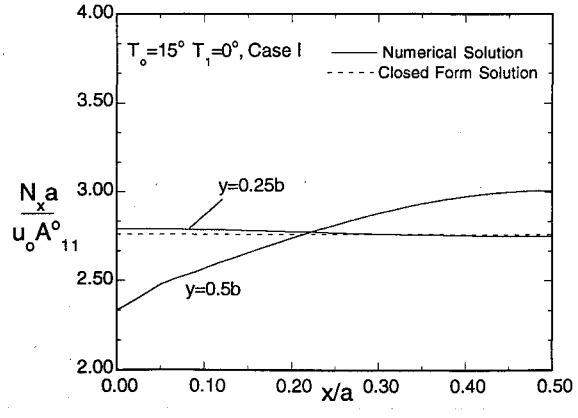

Fig. 6 Axial stress resultant for a panel with a 15 deg angle change.

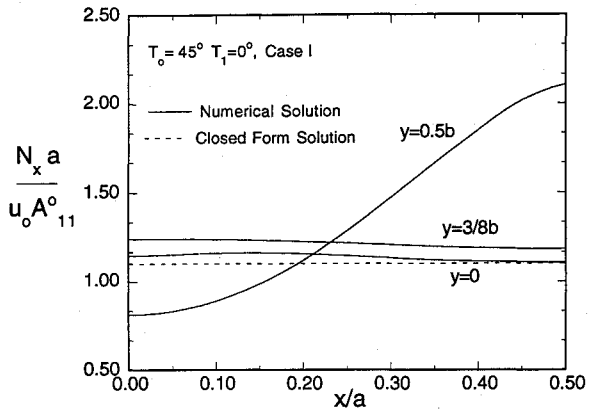

Fig. 7 Axial stress resultant as a function of x and y.

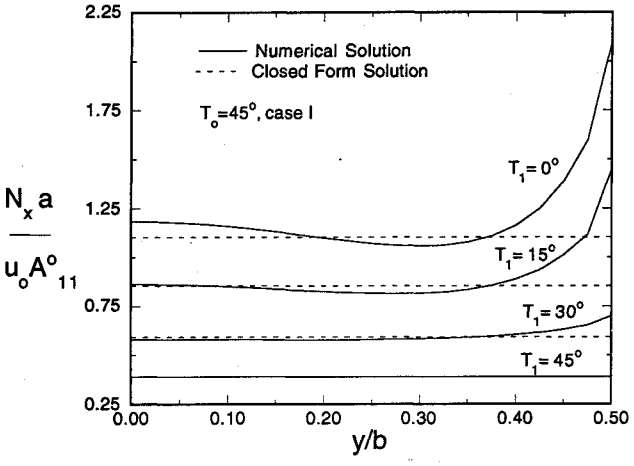

Fig. 8 Axial stress resultant at $x = a/2$ for case I with $T_0 = 45$ deg.

The normalized axial stress resultant N_x for a panel having $T_0 = 15$ deg and $T_1 = 0$ deg is shown in Fig. 6 as a function of the x coordinate for two values of y/b; also shown is the value of N_x obtained from the closed-form solution. The numerically calculated value of N_x changes with respect to both x and y. Note that the closed-form solution accurately predicts N_x at $y = b/4$; for values of y less than $b/4$ the correlation is even better. As the value of y approaches the free edge at $y = b/2$, however, the closed-form solution tends to overestimate the value of N_x at the panel midlength and underestimate it at the panel end. The error at the panel end is 8%.

Variable stiffness panels under uniaxial loading do not have a homogeneous stress state, and the lack of homogeneity depends on the amount of change in the fiber orientation. The closed-form solution, which assumes a homogeneous stress state, will, therefore, be susceptible to large error when large angle changes take place. For example, the variation of N_x is shown in Fig. 7 as a function of the axial coordinate x and the transverse coordinate y for a panel having $T_0 = 45$ deg and $T_1 = 0$ deg. The value of N_x remains nearly constant until the value of y approaches the edge, $y = b/2$. At the edge, the normalized N_x ranges from 0.80 at $x = 0$ to 2.10 at $x = a/2$. Equations (11a) and (11b) help explain this change. Because of a continuously changing fiber orientation, the expansion of the panel due to the Poisson effect will not be uniform; that is, some parts of the panel expand more than others under the compressive load. As a result, shear strains are induced, which give rise to N_{xy}. However, the boundary conditions require that the shear stress resultant be zero at the panel edges and the planes of symmetry. Therefore, large gradients will develop from the middle of the quarter plate to the planes of symmetry and the plate edges. To satisfy the equilibrium equations, an equal and opposite gradient must develop in N_x. The variation of N_x as a function of the y coordinate is shown

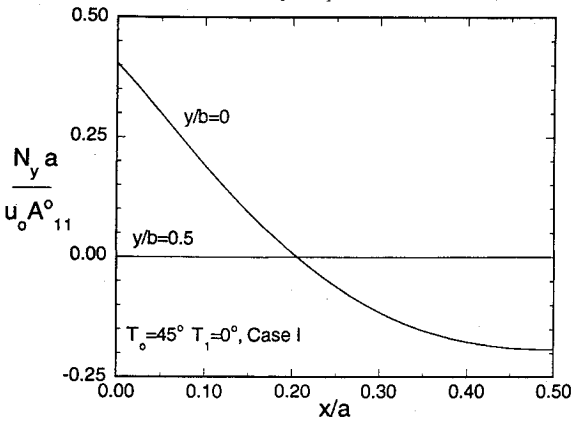

Fig. 9 Transverse stress resultant along x/a (case I).

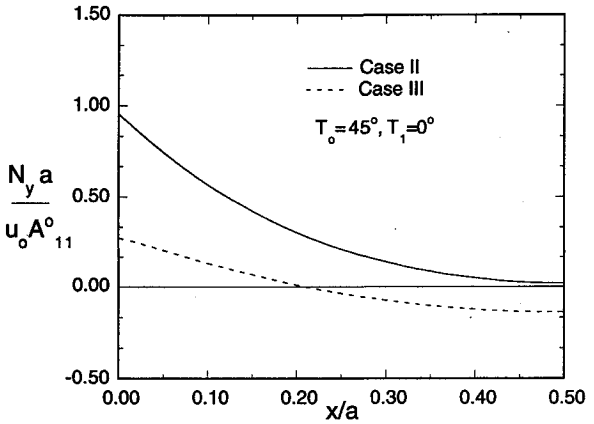

Fig. 10 Transverse stress resultant along x/a (cases II and III).

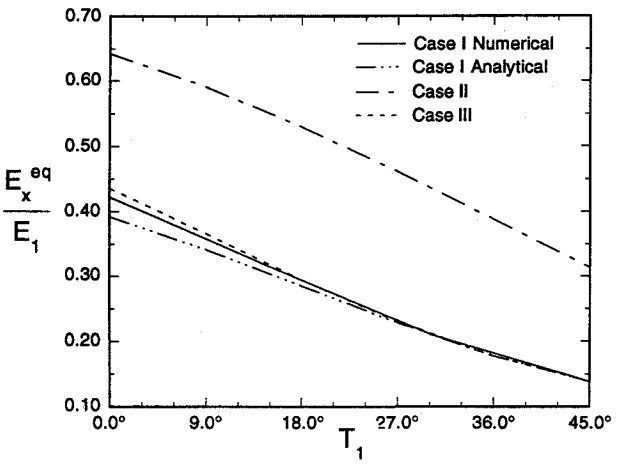

Fig. 11 Panel equivalent stiffnesses.

in Figure 8 for panels having $T_0 = 45$ deg and various values of T_1. For $T_1 = 45$ deg the gradient effect does not appear because the laminate has a straight fiber format. The gradient in N_x close to the transverse edge becomes more pronounced as the difference between T_0 and T_1 increases.

For large angle variations, even though the panel is loaded uniaxially, the value of N_y may become substantial. For a small angle change between T_0 and T_1, its value is two orders of magnitude smaller than N_x, so it may be ignored. The value of N_y, assumed to be zero everywhere for the closed-form solution, is not zero in the interior of the panel. For example, the transverse stress resultant N_y for a panel with $T_0 = 45$ deg and $T_1 = 0$ deg is shown in Fig. 9 as a function of the x coordinate for $y = 0$ and $y = b/2$. Note that at $y = 0$ the value of N_y is of the same order of magnitude as N_x, so its value cannot be neglected. Under compression, the transverse stress resultant at $y = 0$ is compressive for values of x/a less than 0.22 and tensile for greater values. The boundary condition at $y = b/2$ is satisfied, since the value of N_y is indeed zero along that line.

Cases II and III: Fixed and Free-but-Straight Transverse Edges

The analytical solutions that were developed for cases II and III satisfy the boundary and equilibrium conditions exactly. A numerical model of these two cases was also implemented. The results for both cases are nearly exact, with an error of at most 0.04%, introduced due to the discretization of the problem. Therefore, it is concluded that the collocation technique yields valid results in the solution of the equilibrium equations.

The u displacement distribution and, therefore, the axial strain are nonlinear as shown in Fig. 5. As in case I, the axial strain is highest where the panel has a lower stiffness. An interesting result is that the deformation patterns for case I at $y = 0$ and case III are identical, although the boundary conditions are different. However, the patterns are different at $y = b/2$, indicating that in the interior of the panel whether the panel edges remain straight or not has little bearing on the response of the u displacement.

For these two cases, despite the fact that the panels have a variable axial stiffness, the axial stress resultant N_x remains constant. Although the transverse stress resultant N_y changes with respect to x and y for case I, for cases II and III it only varies with x. For both cases the distribution of N_y as a function of x is shown in Fig. 10 when $T_0 = 45$ deg and $T_1 = 0$. When the edges of the panel are immovable (case II), a compressive axial load will give rise to a compressive transverse stress resultant along the entire length. As shown in the figure, close to $x = 0$ the panel will develop a high N_y to counteract the high Poission effect where the fiber angle is 45 deg. In fact, the N_y at $x = 0$ is 50 times larger than at $x = a/2$. For case III, a compressive load will give rise to a transverse stress resultant N_y that is tensile or compressive, depending on the x coordinate. According to Fig. 10, if the panel is given an end shortening u_0, a compressive N_y develops for values of x/a less than 0.22, and a tensile N_y develops if x/a is greater than 0.22. Recall that under the boundary conditions for case III, the total transverse load being applied is zero. Therefore, it may be possible to choose the values of T_0 and T_1 such that the tensile transverse loads develop in the center of the panel when the panel is compressed, thereby preventing the onset of instability.

Overall Panel Stiffness

Engineering applications often require an estimate of the overall stiffness of a structural component. An equivalent panel stiffness E_x^{eq} can be defined as a global quantity for a variable stiffness panel by

$$E_x^{eq} = \frac{Pa}{hbu_0} \tag{41a}$$

where

$$P = \int_0^{b/2} N_x(a/2, y)\, dy \tag{41b}$$

where u_0 is the end shortening of the plate, or $u(a/2, y)$. The value of E_x^{eq} is a measure of the force required to obtain a prescribed displacement at the panel end.

For the three boundary conditions being considered, the relationship between the panel end angle T_1 and the equivalent stiffness is shown in Fig. 11 for a panel with $T_0 = 45$ deg. For case I, the relationship between the equivalent stiffness and the angle T_1 is roughly linear. Decreasing T_1 has the effect of stiffening the panel. But the maximum panel stiffness that can be reached ($T_1 = 0$ deg) is only 42% of the stiffness of a 0-deg straight fiber panel, which has a stiffness of E_1. However,

compared to the stiffness of a 45-deg straight fiber panel, the stiffness of a $T_0 = 45$-deg $T_1 = 0$-deg panel is three times larger. As expected, the curves for the approximate and numerical values converge as the panel approaches the straight fiber format $T_0 = T_1 = 45$ deg. Comparing the stiffness calculated based on the numerical solution and the approximate solution, the maximum difference is 6.5% at $T_1 = 0$ deg and decreases as T_1 approaches T_0. Therefore, the closed-form solution captures the global response and can be used to estimate global stiffness even for large angle changes. For panels with boundary conditions I and III, the global response is nearly identical. For case II, the stiffness is much higher since the panel is constrained in the transverse direction.

Conclusion

The elastic behavior of variable stiffness panels is governed by an elliptic boundary value problem. Unlike panels with straight fibers, the displacement fields and stress resultants are seldom homogeneous. Exact closed-form solutions are obtainable for some sets of boundary conditions, although the common problem of compression with free transverse edges requires a numerical solution. Hermite collocation was found to perform well in the solution of the in-plane problem when the transverse edges are free to deform. The closed-form solution developed for this case may be used when the angle change is small, and the assumptions under which it was developed still hold true. The results of the numerical model show that changes in the elastic properties will generate stress gradients that give rise to transverse stresses although the transverse edges are not loaded, and to shear even when no material shear-extension coupling is present and the loading is uniaxial. The designer may take advantage of this to tailor the stress distribution over the plate area. For the cases with fixed transverse edges and free-but-straight transverse edges, there is excellent correlation between the numerical solution and the exact solutions. The angles T_0 and T_1 may be chosen to better accommodate a given loading condition, achieve a certain stiffness, or perhaps improve the buckling performance.

Acknowledgments

This work was funded by the NASA Langley Research Center through Grant NAG-1-643. The technical grant monitors are James Starnes and Mark J. Shuart. The authors gratefully acknowledge the financial support. The authors also acknowledge Calvin Ribbens of the Computer Science Department, Virginia Polytechnic Institute and State University, for providing technical assistance with the ELLPACK software.

References

[1]Martin, A. F., and Leissa, A. W., "Application of the Ritz Method to Plane Elasticity Problems for Composite Sheets with Variable Fiber Spacing," *International Journal of Numerical Methods in Engineering,* Vol. 28, No. 8, 1989, pp. 1813–1825.

[2]Kuo, C. M., Takahashi, H., and Chou, T. W., "Effect of Fiber Waviness on the Nonlinear Elastic Behavior of Flexible Composites," *Journal of Composite Materials,* Vol. 22, No. 11, 1988, pp. 1004–1022.

[3]Hyer, M. W., and Lee, H. H., "The Use of Curvilinear Fiber Format to Improve Buckling Resistance of Composite Plates with Central Circular Holes," *Composite Structures,* Vol. 18, No. 3, 1991, 239–261.

[4]DiNardo, M. T., and Lagace, P. A., "Buckling and Postbuckling of Laminated Composite Plates with Ply Dropoffs," *AIAA Journal,* Vol. 27, No. 10, 1989, pp. 1392–1398.

[5] Jones, R. M., *Mechanics of Composite Materials,* Hemisphere, New York, 1975, Sec. 2.7, pp. 57–59.

[6]Sewell, G., *The Numerical Solution of Ordinary and Partial Differential Equations,* Academic Press, San Diego, CA, 1988.

[7]Rice, J. R., and Boisvert, R. F., *Solving Elliptic Problems Using ELLPACK,* Springer-Verlag, New York, 1985, pp. 150–153.

[8]Wolfram, S., *Mathematica: A System for Doing Mathematics by Computer,* Addison-Wesley, New York, 1992.